DOI: 10.1002/asia.200800231

Morphogenesis and Crystallization of ZnS Microspheres by a Soft Template-Assisted Hydrothermal Route: Synthesis, Growth Mechanism, and Oxygen Sensitivity

Liangbao Yang, Jun Han, Tao Luo, Minqiang Li, Jiarui Huang, Fanli Meng, and Jinhuai Liu*[a]

Abstract: Almost monodisperse ZnS microspheres have been synthesized on a large scale by a hydrothermal route, in which tungstosilicate acid (TSA) was used as a soft template. By controlling the reaction conditions, such as reaction temperature, pH value of the solutions, and the reaction medium, almost monodisperse microspheres can be synthesized. The structure of these microspheres is sensitive to the reaction conditions. The growth mechanism of these nearly monodisperse microspheres was examined. Oxygen sensing is realized from ZnS microspheres. The current through the ZnS microspheres under UV illumination increases as the oxygen concentration decreases.

Keywords: hydrothermal synthesis · microspheres · oxygen · sensors · templates

Introduction

As one of the most important semiconductors, zinc sulfide (ZnS) has been known for a long time as a versatile and excellent phosphor host material; it has a wide band gap of 3.88 eV and a small Bohr radius (2.4 nm), which make it an excellent candidate for exploring intrinsic recombination processes in dense excitonic systems. Arising from its high luminous efficiency in direct transitions, ZnS was expected to be an optical semiconductor in the near-ultraviolet region. ZnS nanocrystals with various morphologies have already been synthesized, such as nanowires,[1–3] nanosheets,[4,5] nanobelts,[6,7] nanorods,[8] and nanotubes.[9] Some methods for the preparation of nanocrystalline ZnS include the sonochemical method,[10] microwave irradiation,[11] the sol–gel technique,[12–14] plasma-assisted metal organic chemical vapor deposition,[15] and template methods.[16–25]

The template method is an important route for forming ZnS hollow nanospheres. In previous work, many hollow spheres were synthesized by using hard[16–21] or soft templates.[22–25] In most cases, pure-phase samples were obtained only after removal of the templates. The use of tungstosilicate acid (TSA) ion as a soft template to synthesize nanoparticles is an important method. TSA ions form a subset of polyoxometalates of Keggin structure. It is well known that Keggin ions undergo stepwise multielectron redox processes without a structural change.[26] They may be reduced electrolytically, photochemically, or chemically (with suitable reducing agents). They are a large category of metal oxygen cluster anions with well defined structures and properties, have diverse applications in the fields of analytical chemistry, biochemistry, and solid-state devices, and have been used as antiviral and antitumor reagents. Their redox chemistry is characterized by their ability to accept and release a certain number of electrons in distinct steps without decomposition.[27] Recently, Sastry and co-workers used $[PW_{12}O_{40}]^{3-}$ ions to make phase-pure core–shell nanoparticles.[28] They also used $[PW_{12}O_{40}]^{3-}$ as a template for the in situ growth of metal nanoparticles,[29] star-shaped calcium carbonate crystals,[30] and CdS nanoparticles.[31]

In this work, we use TSA as a soft template for the formation of solid spheres. In the experimental process, we found that TSA played an important role in the formation of ZnS solid nanospheres, and we give a reasonable explanation for this role herein. ZnS has never been used in oxygen sensing, because of its low carrier density and its irreversible reaction with oxygen. However, these problems could be solved by using ultraviolet (UV) illumination. The illumination en-

[a] L. Yang, J. Han, T. Luo, M. Li, J. Huang, F. Meng, J. Liu
The Key Laboratory of Biomimetic Sensing and Advanced Robot Technology
Anhui Province, Institute of Intelligent Machines
Chinese Academy of Science
Hefei, 230031 Anhui (China)
Fax: (+86) 551-5592420
E-mail: jhliu@iim.ac.cn

hances the modulation of conductance by adsorbed oxygen.[32] Herein, we demonstrate an approach to oxygen sensing at room temperature by using ZnS microspheres.

Result and Discussion

Hydrothermal treatment of a dispersion of amorphous particles at 160 °C for 10 h results in the formation of ZnS microspheres with good crystallinity, as shown in the X-ray diffraction (XRD) pattern (Figure 1). All reflection peaks of the products can be indexed as a pure structure with cell parameters $a=b=3.83$ Å and $c=6.26$ Å, which are in good agreement with the literature value (JCPDS card 5-492). Although the diffraction peaks (100) and (101) overlap with the peak (002) owing to widening, the product should be the hexagonal phase. According to Scherrer's equation ($d=k\lambda/\beta\cos\theta$), the mean size of particles is about 12 nm.

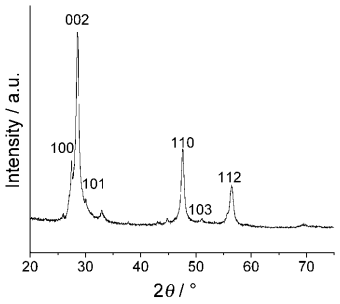

Figure 1. XRD pattern of ZnS sample prepared by aging at 160 °C for 10 h.

Figure 2 A shows the low-magnification SEM image of the as-prepared precipitate, which clearly indicates that the precipitate consists of a large quantity of micrometer-scale spheres. The size distribution of such particles indicates that all these particles are nearly monodisperse with an average diameter of about 1.8 μm. The high-magnification SEM image shown in Figure 2 B reveals that these particles are spherical and that the microparticles tend to form ordered structures. High-magnification SEM images of the surface structures indicate that the surface of the crystal is rough and composed of plenty of nanoparticles with a size of about 20–60 nm (see inset of Figure 2 B). Imaging of broken spheres obtained by ultrasonic treatment (Figure 2 C) confirms that the inner part is also composed of such spherical nanoparticles and that the assembly has a relatively soft nature to allow the mobility of nanoparticles for their rearrangement. A TEM image (Figure 2 D) confirms the uniformity of the microspheres and gives an average diameter of about 1.7 μm. In Figure 2 E, EDAX measurements of drop-coated films of as-prepared precipitate on Cu substrates clearly reveal the presence of Zn and S, suggesting the presence of the microspheres.

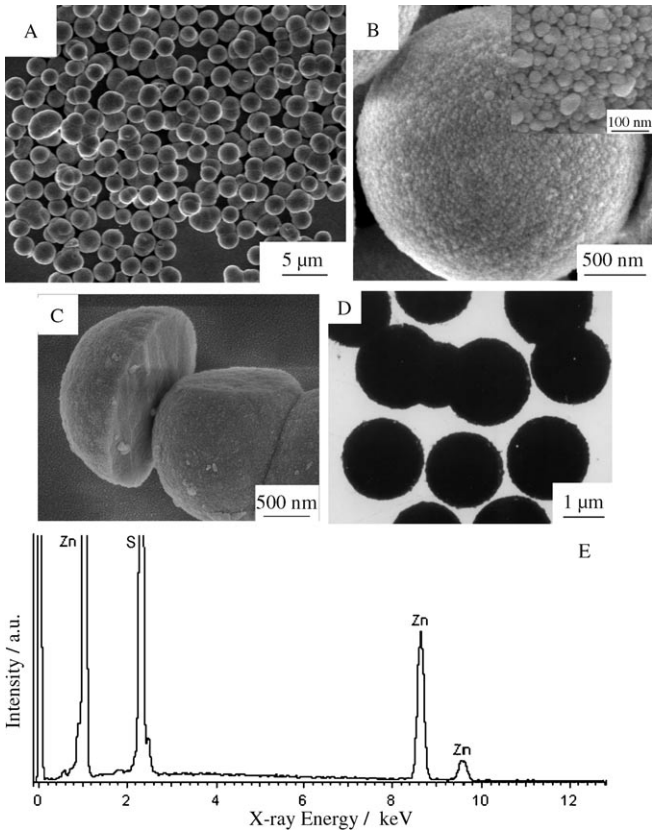

Figure 2. A,B) SEM images of ZnS microspheres at low and high magnification. C) SEM image of ZnS microspheres after ultrasonic treatment. D) TEM image of the ZnS microspheres. E) EDAX spectrum of the as-prepared sample.

The purity and composition of the as-prepared precipitate was examined by using X-ray photoelectron spectroscopy (XPS). Figure 3 A shows a survey spectrum of the product.

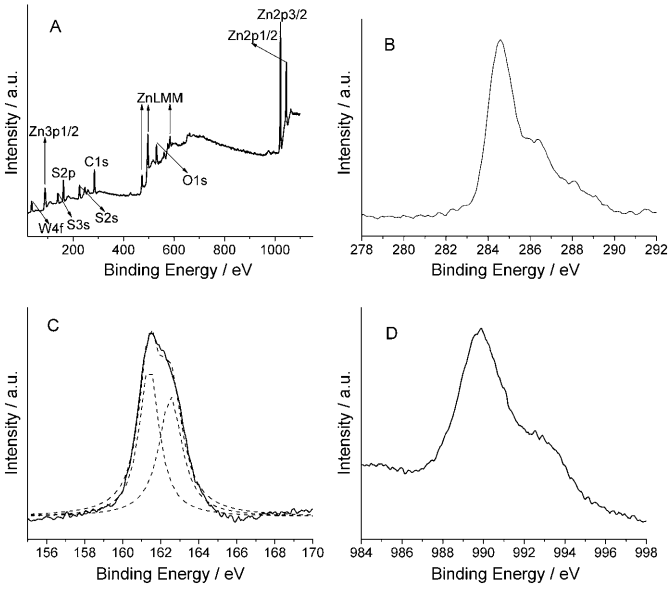

Figure 3. XPS spectra of product: A) survey spectrum, and B) C1s, C) S2p, D) ZnLM2 regions.

The Zn, S, C, and O peaks can be clearly observed. Figure 3B shows the C 1s peak. The binding energies obtained were corrected for specimen charging by reference to C 1s at 285 eV. Figure 3C shows the multiplex spectrum of sulfur peaks. The peaks at binding energies of 161.37 and 162.56 eV can be assigned to S 2p3/2 and S 2p1/2 of the Zn–S bond, respectively.[33] Moreover, the atom ratio of Zn/S is about 1. The signal at 989.88 eV can be attributed to the kinetic energy of ZnLM2 (shown in Figure 3D). The only existence mode of zinc is the ZnS compound combining the ZnLM2 kinetic energy and Zn 2p3/2 binding energy identified at 1020.98 eV (Figure 3A). The XPS analysis results are well in accord with XRD analysis and EDAX measurements.

To understand better the formation of large, spherical ZnS particle assemblies, the kinetics of crystallization was monitored as a function of aging time for the hydrothermal process. Figure 4 shows representative SEM micrographs recorded for aging times of 0.5 (A), 1 (B), 2 (C), and 10 h (D). Figure 4A shows that there are plenty of particles with a size of several nanometers. The larger particles could grow from the smaller ones during the hydrothermal treatment. After aging for 1 h, the particles have already grown to about micrometer size, and there is evidence of the final spherical structure. There are also many ellipsoid structures (Figure 4B). After aging for 2 h, a very large percentage of the particles have grown, and the number of ellipsoidal particles have decreased (Figure 4C). From this image, it appears that the growth of the ZnS crystallites proceeds from within the precursor small particles and leads to their assembly on the surface of the precursor small particles. After aging for 10 h, the particles have evolved considerably in size and shape (Figure 4D), and exhibit a distinct and highly regular morphology. The overall morphology of the particles undergoes a clear resemblance to the final spherical morphology.

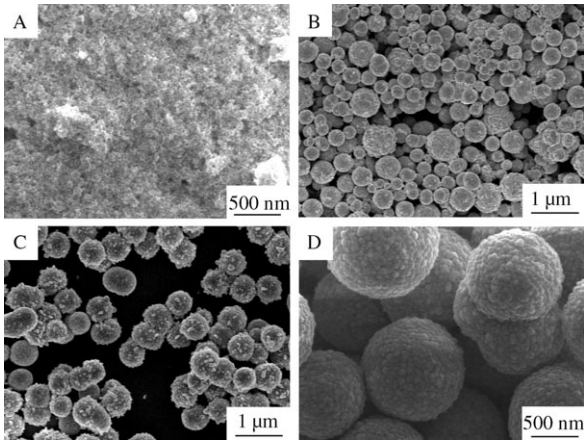

Figure 4. SEM images of ZnS microspheres synthesized with treatment times of A) 0.5 h; B) 1 h; C) 2 h; and D) 10 h.

TSA also played an important role in the formation of the spherical particles of ZnS. Figure 5 shows SEM images of ZnS synthesized by a hydrothermal treatment with different concentrations of TSA. A comparative experiment was performed under the same conditions, but without TSA: there were no spherical nanoparticles in the products (Figure 5A). When the concentration of the TSA was very low, some distorted spherical particles were obtained (Figure 5B). When the experiment was performed with the appropriate concentration of TSA, plenty of regular spherical ZnS particles were formed (Figure 5C). All of these results indicated that TSA plays an important role in the reaction and assembly processes.

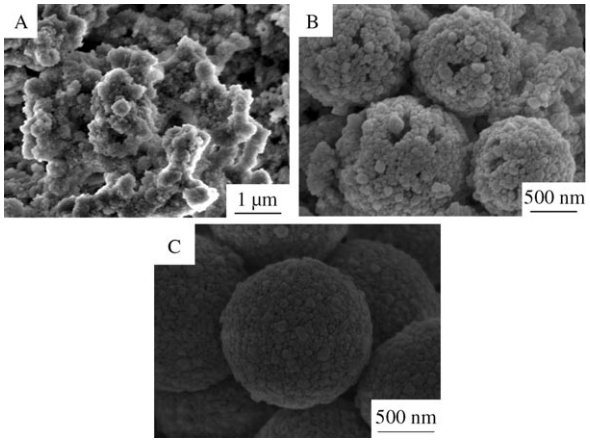

Figure 5. SEM images of ZnS synthesized by hydrothermal treatment with concentrations of TSA of A) 0; B) 10^{-4} M; and C) 10^{-3} M.

Possible chemical reactions involved during the hydrothermal treatment are shown in Equations (1) and (2).

$$2\,Zn^{2+} + [SiW_{12}O_{40}]^{4-} \rightleftharpoons Zn_2[SiW_{12}O_{40}] \quad (1)$$

$$Zn_2[SiW_{12}O_{40}] + 2\,CH_3CSNH_2 + H_2O \rightarrow 2\,ZnS\downarrow + CH_3CN + HAc + [SiW_{12}O_{40}]^{4-} \quad (2)$$

The two reactions in such a system [Eqs. (1) and (2)] occur competitively. Because the solubility of $Zn_2[SiW_{12}O_{40}]$ is far larger than that of ZnS, $Zn_2[SiW_{12}O_{40}]$ crystals are not formed. Therefore, ZnS is the dominant end product. These possible chemical reactions agree with the conclusions of the XPS spectra (Figure 3) and the XRD pattern (Figure 1).

A reasonable route for the growth of the ZnS microspheres, on the basis of the obtained results, is shown in Scheme 1. In solution, TSA ions are clusters.[28] On electrostatic grounds, the clusters are spherical. In step 1, strong interaction between the Zn^{2+} cations and the TSA anion leads to the formation of spherical Zn–TSA colloidal particles. In step 2, when the CH_3CSNH_2 solution is added to the precursor Zn–TSA, TSA ions are replaced by S^{2-} to form ZnS, because the solubility of ZnS is far less than that of TSA. This step is the nucleation and growth step. Generally,

CHEMISTRY
AN ASIAN JOURNAL

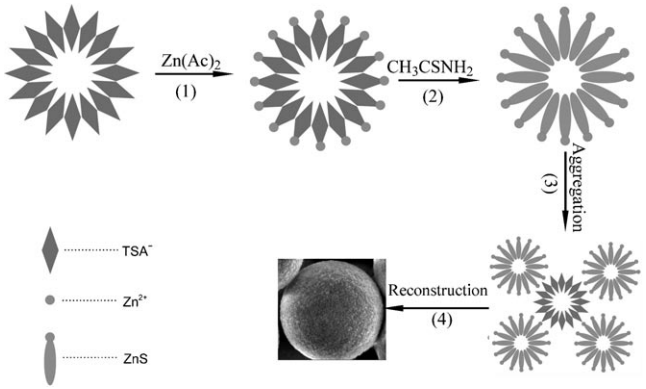

Scheme 1. The formation process of ZnS microspheres.

van der Waals forces are believed to drive the aggregate growth of nanostructures.[34] These observations suggest an assembly process as illustrated in steps 3 and 4. First, small spherical ZnS particles adsorb on the surface of TSA cluster ions to form larger particles held together by electrostatic forces. Then these larger particles aggregate into microspheres in solution. In fact, primary nanoparticles and larger particles of different sizes undergo restructuring or rearranging into a more compact/dense microparticle texture. TSA keeps the primary nanoparticles and then the larger particles slightly apart, and may provide them with a moderate degree of mobility to regulate their position in the aggregate, which is typically thought to occur in the process of oriented attachment of biomineralization.[35] As reported earlier,[30] uniform crystalline particles form from the template-directed aggregation of small particles and subsequent reconstruction rather than simple aggregation of small particles (shown in step 4). In the whole process, TSA ions play an important role (soft template) in affecting the final morphology of the ZnS particles, which is in agreement with the results of our experiments (see Figures 4 and 5).

To understand the kinetics of crystallization better, the XRD pattern was monitored as a function of aging time for the hydrothermal treatment process. Figure 6 shows the time-dependent phase transformation and transition under the present conditions. At the early stages of the reaction (Figure 6a and b), cubic-phase ZnS nanospheres were produced. After a reaction time of 6 h (Figure 6c and d), hexagonal nanospheres were obtained. The evolution from the cubic phase to the hexagonal phase with greater reaction time is shown in Figure 6. At the same time, we observed the growth of diffraction peaks of (100), (101), and (103), although the evolution process of (002), (110), and (112) diffraction peaks cannot be seen because they overlap with the peaks for (111), (220), and (311), respectively, of the cubic phase. All of these results are similar to the work of Liu et al.[23] The reason for this similarity is not clear at present, but we might consider that the different reaction times lead to different ZnS nanoparticle packing modes. Short reaction time is favorable for cubic-phase ZnS formation, whereas long reaction time is suitable for the formation of hexagonal-phase ZnS.

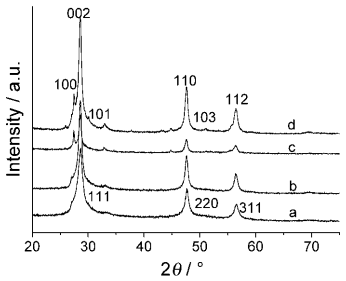

Figure 6. XRD patterns recorded from drop-coated films on Si(111) substrates of ZnS synthesized for reaction times of a) 1 h; b) 3 h; c) 6 h; and d) 10 h.

To produce different structures of ZnS microspheres, we carefully examined the influence of several parameters such as temperature, pH value, and reaction media. Figure 7 shows that the surface structure of the microspheres varies with different reaction temperatures. When the reaction temperature was 65 °C, microspheres with a diameter of about 1.5 μm were obtained (Figure 7A). Each microsphere is composed of many loosely aligned nanoflakes (Figure 7B). When the temperature was increased to 110 °C, the average diameter of spheres was around 1.2 μm (Figure 7C). Interestingly, the high-magnification SEM image in Figure 7D shows a highly spherical assembly of primary nano-

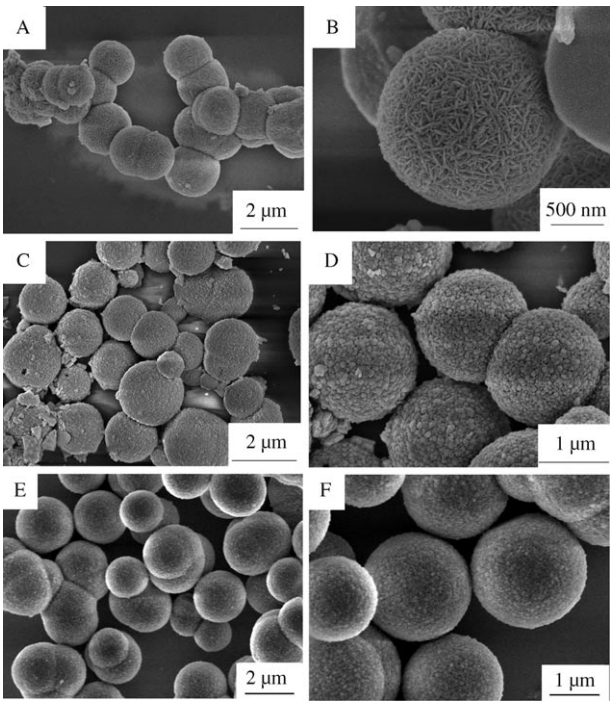

Figure 7. SEM images of the ZnS nanoparticles synthesized by hydrothermal treatment at different temperatures. A) low magnification, 65 °C; B) high magnification, 65 °C; C) low magnification, 110 °C; D) high magnification, 110 °C; E) low magnification, 160 °C; F) high magnification, 160 °C.

particles. Each of these microspheres with a size of 1.2 μm consists of about half a million nanoparticles with sizes of 20–40 nm. When the temperature was kept at 160 °C, the average diameter of the spheres was 1.7 μm, and the surface of the particles became relatively smooth (Figure 7 E and F).

The pH value also plays an important role in the process. Well-crystalline monodisperse microspheres can be obtained at 160 °C only at a pH value of about 2.5 (Figure 8 A). When the pH value was increased to 3.5, some nanoparticles appeared (Figure 8 B), which tended to aggregate together to

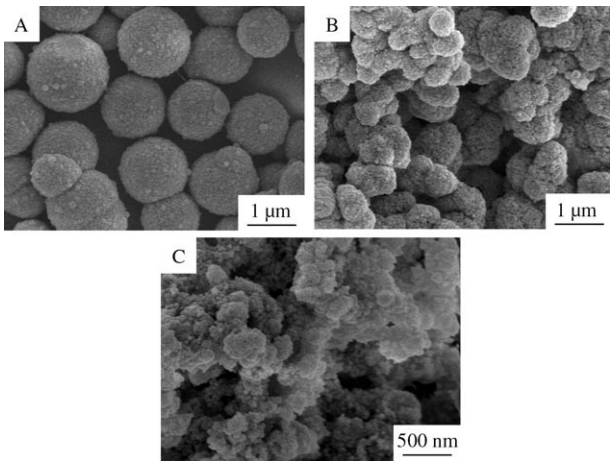

Figure 8. SEM images of the ZnS nanoparticles synthesized at different pH values. A) pH 2.5; B) pH 3.5; C) pH 4.5.

form spherical aggregates. Irregular aggregates were found when the pH value of the reaction system was 4.5 (Figure 8 C).

Water and ethanol have been applied as the reaction media for the crystallization of ZnS. ZnS samples obtained from different types of solvent mixtures are shown in Figure 9. In pure ethanol, the ZnS particles are mostly aggregates of oblong blocks with small particles (Figure 9 A). Nearly spherical aggregates and spherical particles were obtained from a mixture of ethanol and H_2O (Figure 9 B); the size of these particles was about 1.2 μm. Quite uniform microspheres with rough surfaces and a broader size range (average diameter of about 1.8 μm) were obtained from an aqueous medium (Figure 9 C). These results demonstrate that a mixture of solvents can provide an effective tool for controlled morphogenesis of ZnS.

To investigate the oxygen-sensing properties of ZnS microspheres, electrically contacted ZnS microspheres were fabricated by dropping sample solutions onto 15 nm thick comblike gold electrodes on silicon substrates with a 400 nm oxide layer on top. The separation between two electrodes was about 25 μm. An SEM image of a typical device is shown in Figure 10. The inset shows ZnS particles between the two gold electrodes. UV illumination was provided by a UV lamp ($\lambda = 254$ nm, power 15 W) fixed at a distance of

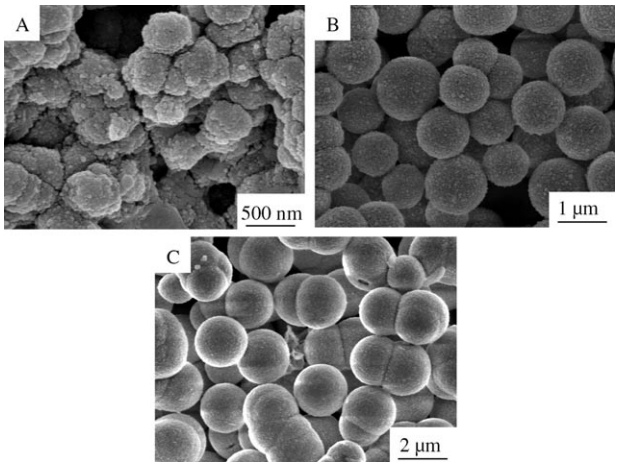

Figure 9. SEM images of the ZnS nanoparticles synthesized in different reaction media. A) C_2H_5OH; B) C_2H_5OH/H_2O (1:1); C) H_2O.

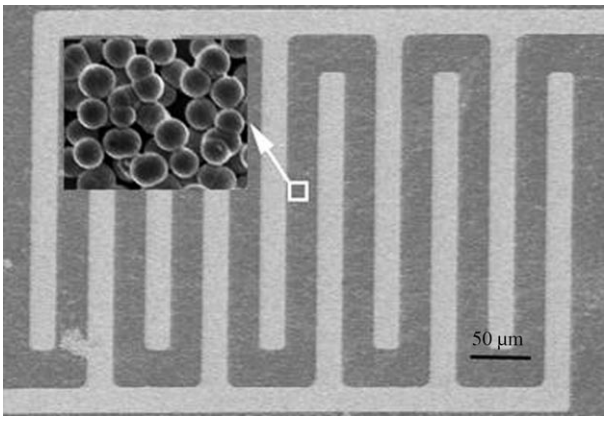

Figure 10. SEM image of the ZnS microspheres placed onto comblike gold electrodes on a silicon (400 nm oxide) substrate. The scale bar is about 50 μm. The ZnS microsphere sample is the same as in Figure 2 A. The inset shows ZnS particles between the two gold electrodes.

10 cm. All measurements were carried out at room temperature.

Figure 11 shows the response of the ZnS microsphere device to different oxygen pressures with or without UV illumination. The measurement was first performed under an oxygen concentration of 600 ppm (Figure 11 A). The current

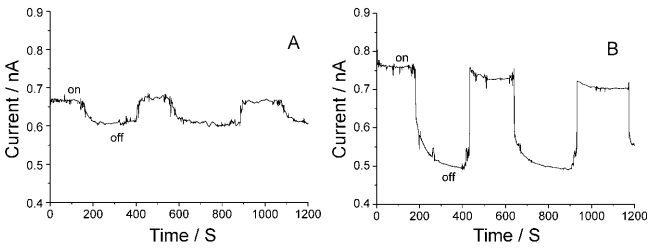

Figure 11. Three cycles of switching between low- and high-conductance states in the presence of oxygen concentrations of 600 ppm (A) and 50 ppm (B) and an applied bias voltage on the microspheres of 10 V.

CHEMISTRY
AN ASIAN JOURNAL

increased from 0.50 to 0.57 nA in 5 s. When the oxygen concentration was decreased to 50 ppm, the current increased to 0.73 nA (Figure 11 B). When the light was turned off, the current recovered to the original dark level within several seconds. Figure 11 also shows three cycle of switching between low and high conductance states with no obvious decay of conductance. It is evident that the microspheres can be reversibly switched between low and high conductance. Since the data were obtained from the interval between two neighboring measurements, the recovery time was below the detection limit of the equipment. The fast response and rapid recovery arose from the generation and recombination of the electron-hole pairs in ZnS.[36] The UV light has a photon energy of 4.9 eV above the band gap of ZnS (3.88 eV). The electron holes are generated by the illumination. Oxygen sensing can be explained by considering a complex process of electron-hole generation, recombination, and adsorption on the surface of the microspheres. When ZnS microspheres are exposed to UV illumination, the carrier density increases because of the generation of electron-hole pairs. This behavior can be explained by simply considering oxygen ions (O^-, O^{2-}, or O_2^-) on the surface of the ZnS microspheres. The oxygen ions capture the photoexcited holes, which liberates the oxygen species and leads to both an enhanced carrier density in the spheres and a narrower depletion width.[37] The amount of the surface oxygen species on the ZnS microspheres at an oxygen concentration of 50 ppm is much smaller than that for a concentration of 600 ppm. Moreover, without UV illumination, only thermally excited holes are available to liberate the adsorbed oxygen from the surface of ZnS microspheres; the low carrier concentration in ZnS limits the modulation of conductance by oxygen.[36] This can explain the slight change of the current of the ZnS microspheres in the absence of illumination.

Conclusions

In conclusion, nearly monodisperse ZnS microspheres can be synthesized by a soft template-assisted solution method. The diameters of these microspheres can be tuned by controlling the reaction conditions. The uniform crystalline particles form from the template-directed aggregation of small particles and subsequent reconstruction. TSA ions act as a template in the complete process. An approach to realize room-temperature oxygen sensing was demonstrated by using synthesized microspheres. The results confirmed that the modulation of conductance was greatly enhanced by adsorbed oxygen under illumination.

Experimental Section

Tungstosilicate acid [$H_4SiW_{12}O_{40}$, TSA], zinc acetate ($Zn(Ac)_2$), and thioacetamide were all A.R. grade and obtained from Shanghai Reagent Co. All reagents in the experiment were used as received.

In a typical experiment, a 1 mM aqueous solution of $Zn(Ac)_2$ (20 mL) was added to a 1 mM aqueous solution of TSA (20 mL) under continuous stirring for 20 min. Thioacetamide (1.2 g) was then introduced. After stirring for 30 min, the mixed solution was transferred into an autoclave with an inner lining of teflon and maintained at 160 °C for 10 h and then allowed to cool to room temperature. The obtained precipitates were centrifuged, washed several times with distilled water and absolute ethanol, and dried in a vacuum at 60 °C for 6 h. The process of the corresponding control experiments was similar to above experiments. The samples for electrical measurement were prepared by depositing a drop (5 μL) of the ZnS solution onto the surface of comblike gold electrodes.

XPS measurements of a film of the sample were carried out on a VG ESCALAB MKII instrument at a pressure greater than 10^{-6} Pa. The general scan and C_{1s}, Ag_{3d}, P_{2p}, and N_{1s} core-level spectra were recorded with non-monochromatized MgK_α radiation (photon energy = 1253.6 eV). The core-level binding energies were aligned with respect to the C_{1s} binding energy of 285 eV. Samples for TEM analysis were prepared by drop-coating films of the solution on carbon-coated copper TEM grids, allowing the grid to stand for 2 min, and then removing excess solution with blotting paper. TEM analysis was carried out on a JEM model 100SX electron microscope (Japan Electron Co.) operated at an accelerating voltage at 200 kV. SEM measurements were carried out with a Leica Stereoscan-440 instrument equipped with a Phoenix energy-dispersive analysis of X-rays (EDAX) attachment. XRD analysis of drop-coated films of the sample solutions on silicon substrates was carried out on a MAP18AHF instrument (Japan MAC Science Co.).

Two-terminal two-probe current measurements were made by using a picoammeter/voltage source (Keithley 6487) in the range 0–500 V. The dc current sensitivity of the system is of the order 10^{-14} A. Timed data acquisition was performed by using a LabView program, and the current sampling frequency was set at two samples per second. The bias voltage was set at $V = 10$ V in all of the experiments.

Acknowledgements

The financial support of this work by the National Basic Research Program of China (2007CB936603) and the National Science Foundation of China (project Nos. 60574095 and 60574094) is gratefully acknowledged.

[1] Y. Wang, L. Zhang, C. Liang, G. Wang, X. Peng, *Chem. Phys. Lett.* **2002**, *357*, 314–318.
[2] X. M. Meng, J. Liu, Y. Jiang, W. W. Chen, C. S. Lee, I. Bello, S. T. Lee, *Chem. Phys. Lett.* **2003**, *382*, 434–438.
[3] D. F. Moore, Y. Ding, Z. L. Wang, *J. Am. Chem. Soc.* **2004**, *126*, 14372–14373.
[4] S. H. Yu, M. Yoshimura, *Adv. Mater.* **2002**, *14*, 296–300.
[5] J. Li, Y. Xu, D. Wu, Y. Sun, *Solid State Commun.* **2004**, *130*, 619–622.
[6] Y. K. Liu, G. C. Xi, S. F. Chen, X. F. Zhang, Y. C. Zhu, Y. T. Qian, *Nanotechnology* **2007**, *18*, 285605.
[7] Y. F. Hao, G. W. Meng, Zh. L. Wang, Ch. H. Ye, L.D . Zhang, *Nano Lett.* **2006**, *6*, 1650–1655.
[8] J. Xu, Y. Li, *J. Colloid Interface Sci.* **2003**, *259*, 275–281.
[9] X. Wang, P. Gao, J. Li, C. J. Summers, Z. L. Wang, *Adv. Mater.* **2002**, *14*, 1732–1735.
[10] X. H. Liao, J. J. Zhu, H. Y. Chen, *Mater. Sci. Eng. B* **2001**, *85*, 85–89.
[11] J. J. Zhu, M. Zhou, J. Xu, X. Liao, *Mater. Lett.* **2001**, *47*, 25–29.
[12] A. K. Verma, T. B. Rauchfuss, S. R. Wilson, *Inorg. Chem.* **1995**, *34*, 3072–3078.
[13] S. Yanagiya, Y. Iseki, T. Kaito, A. Mori, C. Kaito, T. Sekiguchi, T. Inoue, *Mater. Chem. Phys.* **2007**, *105*, 250–252.
[14] L. H. Dong, Y. Chu, Y. P. Zhang, *Mater. Lett.* **2007**, *61*, 4651–4654.
[15] Q. J. Feng, D. Z. Shen, J. Y. Zhang, H. W. Liang, D. X. Zhao, Y. M. Lu, X. W. Fan, *J. Cryst. Growth* **2005**, *285*, 561–565.

[16] W. H. Zhang, J. L. Shi, H. R. Chen, Z. L. Hua, D. S. Yan, *Chem. Mater.* **2001**, *13*, 648–654.
[17] K. P. Velikov, A. V. Blaaderen, *Langmuir* **2001**, *17*, 4779–4786.
[18] M. L. Breen, A. D. Donsmore, R. H. Pink, S. Q. Qadri, B. R. Ratna, *Langmuir* **2001**, *17*, 903–907.
[19] Z. B. Lei, J. M. Li, Y. X. Ke, Y. G. Zhang, H. C. Zhang, F. Q. Li, J. Y. Xing, *J. Mater. Chem.* **2001**, *11*, 2930–2933.
[20] S. Chah, J. H. Fendler, J. Yi, *J. Colloid Interface Sci.* **2002**, *250*, 142–148.
[21] S. B. Han, X. Y. Shi, F. M. Zhou, *Nano Lett.* **2002**, *2*, 97–100.
[22] X. Jiang, Y. Xie, J. Lu, L. Zhu, W. He, Y. Qian, *Chem. Mater.* **2001**, *13*, 1213–1218.
[23] H. J. Liu, Y. H. Ni, M. Han, Q. Liu, Z. Xu, J. M. Hong, X. Ma, *Nanotechnology* **2005**, *16*, 2908–2912.
[24] X. W. Zheng, Y. L. Xie, Y. Zhu, X. C. Jiang, A. H. Yan, *Ultrason. Sonochem.* **2002**, *9*, 311–316.
[25] A. M. Collins, C. Spickermann, S. Mann, *J. Mater. Chem.* **2003**, *13*, 1112–1114.
[26] V. Kogan, Z. Izenshtat, R. Neumann, *Angew. Chem.* **1999**, *111*, 3551–3554; *Angew. Chem. Int. Ed.* **1999**, *38*, 3331–3334.
[27] "Heteropoly and Isopoly Oxymetalates": M. T. Pope in *Inorganic Chemistry Concepts*, *Vol. 8*, Springer Verlag, Berlin, **1983**, p. 101.
[28] S. Mandal, P. R. Selvakannan, R. Pasricha, M. Sastry, *J. Am. Chem. Soc.* **2003**, *125*, 8440–8441.
[29] A. Sanyal, S. Mandal, M. Sastry, *Adv. Funct. Mater.* **2005**, *15*, 273–280.
[30] D. Rautaray, S. R. Sainkar, M. Sastry, *Langmuir* **2003**, *19*, 10095–10099.
[31] S. Mandal, D. Rautaray, A. Sanyal, M. Sastry, *J. Phys. Chem. B* **2004**, *108*, 7126–7131.
[32] A. S. Zuruzi, A. Kolmakov, N. C. MacDonald, M. Moskovits, *Appl. Phys. Lett.* **2006**, *88*, 102904.
[33] N. Du, H. Zhang, B. D. Chen, J. B. Wu, D. Yang, *Nanotechnology* **2007**, *18*, 115619.
[34] Z. P. Zhang, D. M. Gao, H. Zhao, C. G. Xie, G. J. Guan, D. W. Wang, S. H. Yu, *J. Phys. Chem. B* **2006**, *110*, 8613–8618.
[35] R. Penn, L. Banfield, *Science* **1998**, *281*, 969–971.
[36] Y. G. Liu, P. Feng, X. Y. Xue, S. L. Shi, X. Q. Fu, C. Wang, Y. G. Wang, T. H. Wang, *Appl. Phys. Lett.* **2007**, *90*, 042109.
[37] Q. H. Li, Q. Wan, Y. X. Liang, T. H. Wang, *Appl. Phys. Lett.* **2004**, *84*, 4556–4558.

Received: June 6, 2008
Revised: July 15, 2008
Published online: September 26, 2008

